Rev.Adv.Mater.Sci. 6 (2004) 150-161

GMR AND SOFT MAGNETIC PROPERTIES OF Ni-Mn ALLOYS WITH DISPERSED FERROMAGNETIC NANO PARTICLES

T. Okazaki[1], T. Miyanaga[1], Y. Sakisaka[1], S. Sugimoto[2], K. Yamada[3] and Z. Honda[3]

[1] Faculty of Science and Technology, Hirosaki Univ., Hirosaki 036-8561, Japan
[2] Graduate School of Engineering, Tohoku Univ., Sendai 980-8579, Japan
[3] Dept. Materials Sciences, Saitama University, Saitama 338-8570, Japan

Received: February 27, 2004

Abstract. GMR and soft magnetic properties were investigated in nano-scale inhomogeneous $Ni_{1-x}Mn_x$ alloys (x = 0.20~0.30), where ordered single-domain particles are distributed in disordered nonmagnetic or Ni-rich or Mn-rich matrices. The GMR of Ni_3Mn alloy depends on the volume fraction of ordered domains ε. Maximum value of -1.8% is obtained at $\varepsilon \sim 0.2$. Moreover, the GMR depends remarkably on x: GMR for $0.20 \leq x \leq 0.24$ is small (Type I) and for $0.26 \leq x \leq 0.30$ has a maximum of –6% at $x = 0.30$ (Type II). Types I and II are caused respectively by ferromagnetic and antiferromagnetic interactions between domains.

1. INTRODUCTION

In the Ni_3Mn alloy system, the Cu_3Au-type ordered phase shown in Fig.1 is formed after suitable heat treatment. The most striking characteristic of this system is as follows: a change in the degree of the long-range order causes a wide variety of the magnetic and transport properties. Many studies of Ni_3Mn have been reported so for which concentrate mainly on the completely ordered and disordered states [1-7].

The difference in their texture was observed by Taoka [8] and Marcinkowski and Poliak [9] using transmission electron microscopy. For Ni_3Mn alloys annealed in the temperature range of 733-773K, they demonstrated that the ordered ferromagnetic domains are distributed in a disordered nonmagnetic matrix. In previous study [10, 11], we reported that the value of M for Ni_3Mn annealed at 693K depends on the atomic short-range order. The alloy reveals a superparamagnetic behavior in a wide temperature range above the Curie point T_F , where the alloy has low degree of order. The magnetic analysis based on a superferromagnetic model [12,13] shows that long-range-ordered magnetic domains with nanometer size are distributed in a disordered nonmagnetic matrix.

Giant magnetoresistance (GMR) was observed in a variety of magnetic granular alloy system such as Co-Cu [14], Co-Ag [15] and Fe-Cr [16,17], where single-domain ferromagnetic particles are embedded in a immiscible medium. The GMR in granular systems is due to the additional scattering by ferromagnetic single domain particles, which are randomly oriented. The spin-dependent scattering decreases when the magnetization of particles in superparamagnetic phase is tilted in the direction of the applied field.

In such an inhomogeneous phase, nano-particles are in contact with each other forming a group, where spontaneous magnetization *Ms* of particles has a tendency to be parallel with each other because of exchange interaction. Since each *Ms* in a group have magnetization ripple [18], the system is expected to show soft magnetic property [19].

Corresponding author: T. Okazaki, e-mail:teiko28@cc.hirosaki-u.ac.jp

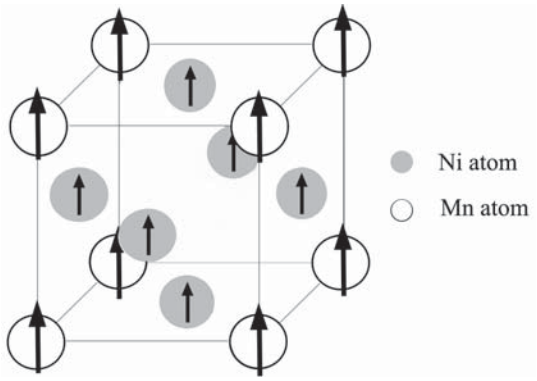

Fig. 1. Ni_3Mn alloy with the Cu_3Au-type ordered phase.

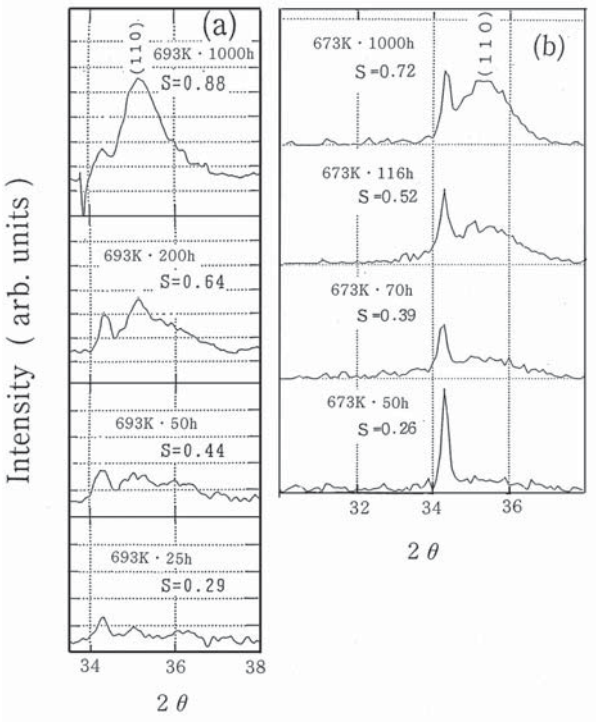

Fig. 2. The (110) $K_{\alpha 1}$ peaks obtained from Ni_3Mn in various ordered states. The *S* is long-range order parameter.

At first, we report about ferromagnetic particle size, magnetization and GMR for Ni_3Mn alloy with various long-range order [20]. Next, GMR and soft magnetic properties of $Ni_{1-x}Mn_x$ (x = 0.20 – 0.30) alloys which have nano - scale inhomogeneity are investigated [21-23].

2. EXPERIMENTAL PROCEDURE

$Ni_{1-x}Mn_x$(x = 0.20 – 0.30) alloys were melted in an rf induction furnace and then cast. These ingots were homogenized by holding in a vacuum for 15 h at 1273K. It was cold-worked into a ribbon (0.5 mm in thickness) and a wire (Φ = 0.5 mm). They were annealed in Ar for various hours at 673–713K to get ordered states. The X-ray diffraction for sheet samples was measured with Cu-K_α radiation. The loop of magnetization *M* vs. magnetic field *H* was measured by using a vibrating sample magnetometer. Resistivity measurements were made by the 4-terminal method in an electromagnet with a maximum applied field of 10 kOe at room temperature. The magnetoresistance (MR) ratio is defined by the following equation:

$$\text{MR ratio} = \Delta\rho/\rho_0 = (\rho_H - \rho_0)/\rho_0 , \qquad (2.1)$$

where ρ_H and ρ_0 are the resistivities with and without *H*, respectively.

Permeability of wire specimen for 1~500 kHz high frequency was measured by impedance analyzer. In order to investigate antiferromagnetic interaction between ferromagnetic nano-scale particles in Mn-rich matrices, we studied magnetization and MR in large pulse magnetic field up to 16 T at low temperature12K.

3. LONG-RANGE ORDER PARAMETER *S* AND AVERAGE PARTICLE SIZE *D*

Fig. 2 shows (110) $K_{\alpha 1}$ peaks with cutting $K_{\alpha 2}$ obtained for the Ni_3Mn alloys, indicating super-lattice formation. A peak at 2θ = 34.2° is attributed to an instrumental artifact. The long-range-order parameter *S* was determined by comparing the integral intensity of the (110) peak to that of the (220) peak.

Average particle size *D* of samples was determined from the broadening of the X-ray diffraction peak by using the Scherrer's equation,

$$D = 0.9\frac{\lambda}{W\cos\theta}, \qquad (3.1)$$

where λ, *W* and θ denote the wavelength (0.15405 nm) , FWHM (full width at half maxmum intensity) of each (110) peaks and Bragg angle. The values of *S* and *D* are given in Table 1. They are 2.8 to 10 nm for *S* = 0.26 to 0.88 states. The <*m*> in Table 1 is also the average particle size estimated by magnetic analysis [11]. We find that the *D* value is about 1.5 times larger than the corresponding <*m*> value.

Thus these values are of the same order in size. The volume fraction ε of the ordered regions can be evaluated by using the relationship [24] $\varepsilon = S^2/S_{do}^2$, where S_{do} is the long-range-order parameter in the ordered domains. Assuming S_{do}= 1, ε is 0.017 to 0.78 for S = 0.13 to 0.88 states.

Fig. 3 also shows (110) $K_{\alpha 1}$ peaks obtained for the present $Ni_{1-x}Mn_x$ (x = 0.20 – 0.30) alloys annealed for 100 h at 693K. The values of S and D are given in Table 2. The S value increases 0.3 to 0.66 with Mn concentration, x for $0.20 \le x \le 0.26$ and reaches to about 0.7 for $0.26 \le x \le 0.30$. The D value also increases about 4 to 6.7 nm with x. The volume fraction ε in the ordered regions is about 0.1 to 0.5 for S = 0.3 to 0.72 states. They are nearly constant value of 0.5 for $Ni_{1-x}Mn_x$ alloys of $0.26 \le x \le 0.30$.

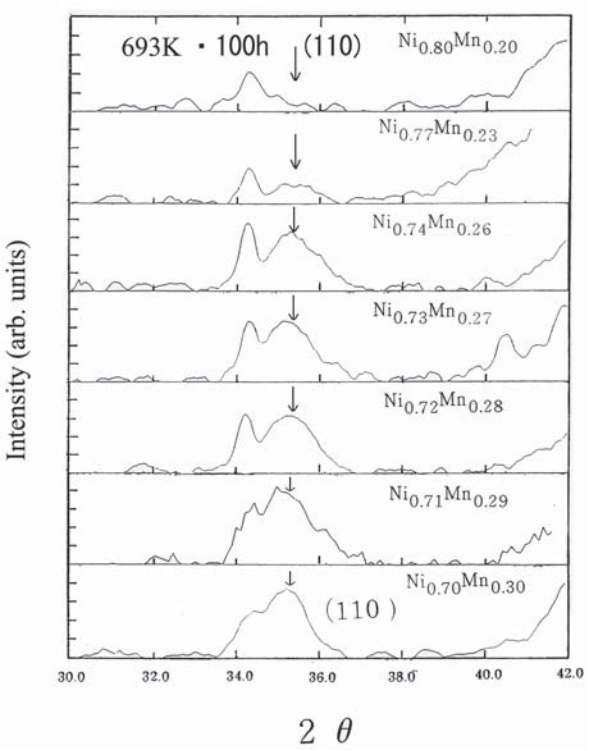

Fig. 3. The (110) $K_{\alpha 1}$ peaks obtained from Ni – Mn alloys annealed for 100 h at 693K.

4. MAGNETIZATION AND GMR OF Ni_3Mn ALLOY

4.1. Magnetization of Ni_3Mn alloy

Fig. 4 shows the M vs. temperature T curves of Ni_3Mn alloys ordered for 5-1000 h at 673K and 693K [10]. The S values in brackets were determined by X-ray diffraction analysis. It was found that M increases sharply with S.

The magnetisum of Ni_3Mn depends on the number n of the nearest-neighbor Mn atoms around an Mn atom [7, 10, 18], because a ferromagnetic interaction operates for the Ni-Ni and Ni-Mn pairs and an antiferromagnetic one for the Mn-Mn pairs. That is, the average exchange interaction around a Mn atom is considered to be $J_{ex} > 0$ for $n < 3$, $J_{ex} \sim 0$ for $n = 3$ and $J_{ex} < 0$ for $n > 3$. The average number $\langle n \rangle$ of n for a Ni_3Mn alloy can be evaluated from S by using Cowley's equation [10,25]. From Fig.1, $\langle n \rangle$ is evaluated to be 0 and ~3, respectively, for the ordered state (S = 1) and the disordered state (S ~ 0). $\langle n \rangle$ decreases with S and M increases with S. It is found that M reaches a maximum of 84 emu/g at S = 0.88 ($\langle n \rangle$ ~ 0.7) for Ni_3Mn ordered at 693K. The value is 82% of one obtained from S = 1 state where the local magnetic moments of $\langle m \rangle_{Ni}$ (~0.31 μ_B) [26] and $\langle m \rangle_{Mn}$ (~ 3.6 μ_B) [26] are parallel to each other.

Table 1. The annealing time (t) at 673K and 693K, the long-range-order parameter (S), average cluster size (D and $\langle m \rangle$), the volume fraction of the ordered regions ($\varepsilon = S^2/S_{do}^2$), ferromagnetic and paramagnetic Curie temperatures T_F(K) and θ_P(K).

	673 K				693 K				
t (h)	50	70	116	1000	5	25	50	200	1000
S	0.26	0.39	0.52	0.72	0.13	0.29	0.44	0.64	0.88
D (nm)	2.8	3.3	3.8	5.9		3.2	4.3	6.5	10
$\langle m \rangle$ (nm)*	1.7	1.8	2.7		1.4	2.1	2.9		
ε	0.068	0.15	0.27	0.52	0.017	0.084	0.19	0.41	0.78
ε*					0.10	0.16	0.32		
T_F (K)	273	353	503	657	241	393	581	713	723
θ_P (K)	482	594	643		550	650	710		

*Ref.[11]

Table 2. The long-range-order parameter (S), average particle size (D) and the volume fraction of the ordered regions($\varepsilon=S^2/S_{do}^2$) for $Ni_{1-x}Mn_x$ alloys (x = 0.20~0.30).

x	S	D (nm)	ε
0.20	~0.3	~4	~0.1
0.23	~0.4	~4	~0.16
0.24	0.44	4.6	0.19
0.26	0.66	4.3	0.44
0.27	0.70	5.1	0.49
0.28	0.66	6.5	0.44
0.29	0.72	6.1	0.52

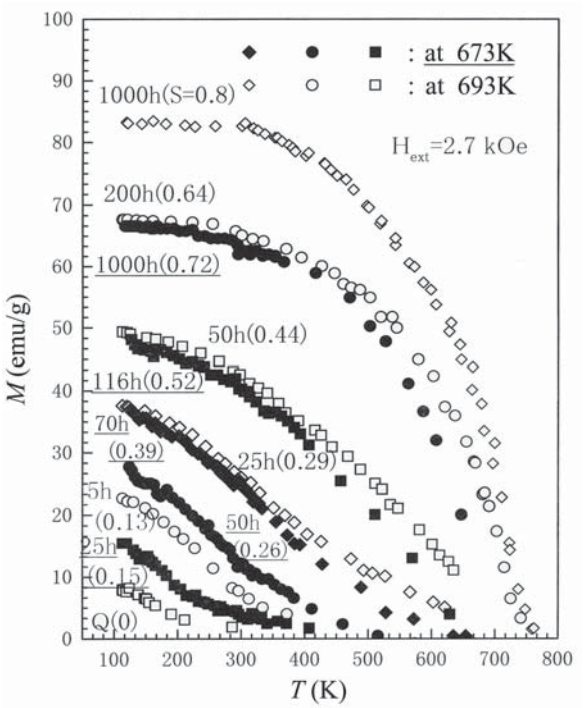

Fig. 4. Magnetization vs. temperature curves of Ni_3Mn alloys ordered for 5 – 1000 h at 673K and 693K. S indicated in brackets is the long-range order parameter.

As seen from the M – T curves in Fig.4, the states for $S \geq 0.64$ are found to be ferromagnetic. The Curie temperature T_F for 673K•1000 h, 693K•200 h and 1000 h states are 657, 713 and 723K, respectively. Furthermore, it should be noted that each curve for $S < 0.64$ states has a long tail in the temperature range of $T > T_F$. We have reported that the magnetism in the range of $T_F < T < \theta_P$ for 693K•5, 25 and 50 h states was superparamagnetic, where θ_P is the paramagnetic Curie temperature. The T_F and θ_P of the 673K•50, 70 and 116 h states, which are determined by Arrott plot and inverse susceptibility vs. temperature curves, are listed in Table 1. For these states also, the magnetism in the temperature range of $T_F < T < \theta_P$ is superparamagnetic, where magnetization of single domain in disordered nonmagnetic matrix orients randomly.

4.2. GMR of Ni_3Mn alloys

Fig. 5 shows the dependence of $\Delta\rho/\rho_0$ // H and $\perp H$ at room temperature on annealing time t at 673 and 693K, where $\Delta\rho/\rho_0$// H and $\perp H$ are the MR ratios for electric current parallel and perpendicular to the applied field, respectively. Since $\Delta\rho/\rho_0$ // H and $\perp H$ are negative for all states except the 673K•25 h state and nearly equal for the annealing time of $t \leq 100$ h, each $\Delta\rho/\rho_0$ is considered to be caused by the GMR effect. The MR ratio for $t \geq 100$ h consists of GMR and anisotropic magnetoresistance (AMR). AMR is caused by ferromagnetic behavior. As all the particles grow and then make a connecting network to form large ferromagnetic domains where the annealing time is longer, the GMR decreases gradually and reaches zero such as in, for example, $\Delta\rho/\rho_0$ //H of the 693K•1000 h state. The effect of GMR is maximized in the 693K•50 h (S = 0.44) and 673K•116 h state (S = 0.52) states.

The finding that the decrease in $\Delta\rho/\rho_0$ // H of 673 K•1000 h is slight suggests that the average size of each domain in 673K•116 h state (D = 3.8 nm) remains nearly constant in the 673K•1000 h state (5.9 nm).

Fig. 6 shows the dependence of the $\Delta\rho/\rho_0$ // H on the volume fraction ε of the ordered regions for the 673K- and 693K- samples. The two $\Delta\rho/\rho_0$ vs. ε curves exhibit a similar tendency, that is, $\Delta\rho/\rho_0 \sim 0$ at $\varepsilon \sim 0$, and $\Delta\rho/\rho_0$ increases sharply at $0 < \varepsilon < 0.1$, reaching a maximum of –1.8% at $\varepsilon \sim 0.27$. Thereafter, it decreases with increasing of ε and returns to zero at $\varepsilon \sim 0.8$. The tendency resembles the dependence of $\Delta\rho/\rho_0$ on the Fe content x in $Cr_{1-x}Fe_x$ granular alloy thin films [16,17]. When these Fe particles of 2.0-3.0 nm in diameter are distributed in Cr matrix at intervals of 5-20 nm, the $\Delta\rho/\rho_0$ has a maximum. The largest effect of spin-dependent scattering in the inhomogeneous phase of Ni_3Mn alloy appears under the condition where ordered domains of ~ 4 nm are distributed in a disordered nonmagnetic matrix at $0.2 < \varepsilon < 0.3$. At D > 6.5 nm, $\varepsilon > 0.4$, as all particles are contiguous with one another form-

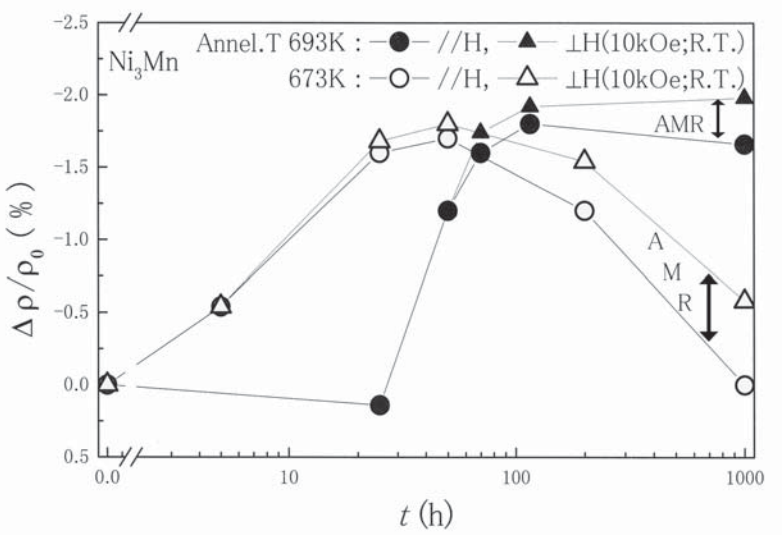

Fig. 5. Dependence of MR ratio $\Delta\rho/\rho_0$ // *H* and $\perp$ *H* at room temperature on annealing time *t* at 673K and 693K. AMR is the anisotropic magnetoresisrance.

ing large ferromagnetic clusters, GMR decreases and disappears in homogeneous ferromagnetic alloys.

4.3. DEPENDENCE OF GMR ON THE MAGNETIC FIELD

If the GMR in granular systems is proportional to the average $<\cos\theta_{ij}>$, where θ_{ij} is the relative angle between the magnetization of two ferromagnetic particles M_i and M_j, the MR raito can be described as [15]

$$\frac{\Delta\rho}{\rho_0} \propto 1 - <\cos\theta_{ij}> = \quad 1 - <\cos\theta_{ij}>^2 = 1 - \left(\frac{M}{M_S}\right)^2, \qquad (4.1)$$

where θ_{ij} denotes the angle between M_i and H, and M and M_S the global and saturation magnetization.

Provided that the GMR in Fig. 5 is caused by spin-dependent scattering on ordered single domains precipitated in a disordered matrix, the dependence of MR ratio on *H* must satisfy equation (4.1).

Fig. 7 shows the dependence of the MR ratio on *H* for (a) 693K•5h and (b) 673K•50h states which have superparamagnetic phase at room temperature. The resistivity decreases with the applied field. For comparison, Fig.7 also shows the theoretical $[1-(M/M_S)^2]$ vs. *H* curves at room temperature, where M_S is obtained by extrapolating the *M*-*H* curve to the value of *H* = 10 kOe. The theoretical curves fit well to the experimental curves, $\Delta\rho/\rho_0$ vs. *H*, for both states in Fig.7.

From the results described above, the GMR in the inhomogeneous phase of a Ni_3Mn alloy is considered to be due to spin-dependent scattering by ferromagnetic particles, and is therefore of the granular type.

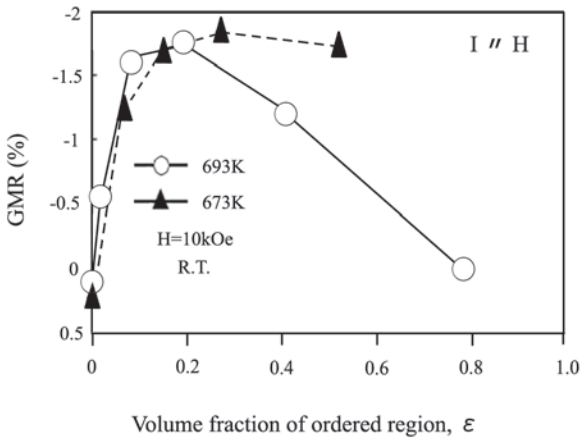

Fig. 6. Dependence of $\Delta\rho/\rho_0$ // *H* on the volume fraction ε of ordered regions, where ε is S^2/S_{do}^2.

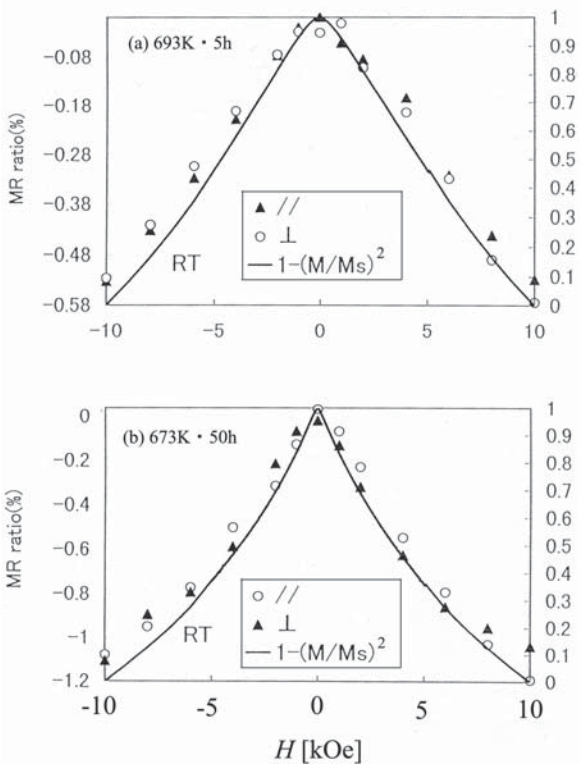

Fig. 7. Dependence of GMR on *H* for (a) 693 K•5h and (b) 673 K•50h states. The solid lines are the theoretical [1- $(M/M_S)^2$] vs. *H* curves, where *M* and M_S are the global and saturation magnetizations.

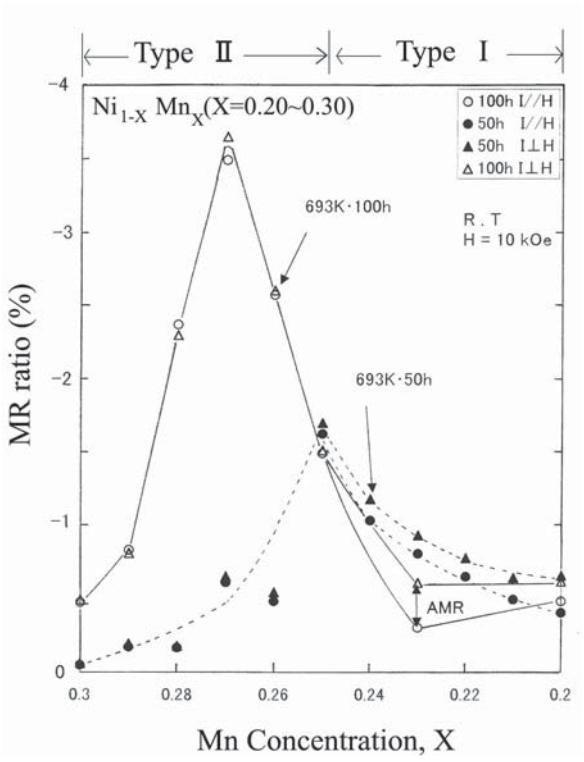

Fig. 8. The dependence of MR ratio for $Ni_{1-x}Mn_x$ (x = 0.20-0.30) alloys on Mn concentration.

5. MAGNETIZATION AND GMR OF $Ni_{1-X}Mn_X$ (x=0.20-0.30) ALLOYS

5.1. GMR of $Ni_{1-X}Mn_X$ (x=0.20-0.30) alloys

From Table 2, we find that the ferromagnetic ordered particles of the size *D* of 4~6.7 nm distribute in a disordered matrix for the present $Ni_{1-x}Mn_x$(x =0.20-0.30) alloys. Fig. 8 shows the dependence of $\Delta\rho/\rho_0$ // *H* and $\perp$ *H* for all samples at room temperature on Mn concentration. Since $\Delta\rho/\rho_0$ // *H* and $\perp$ *H* are negative and nearly equal to each other for $Ni_{1-x}Mn_x$ ($x \geq 0.25$) alloys, each $\Delta\rho/\rho_0$ is caused by the GMR effect. The MR ratio for x<0.25 alloys consists of GMR and anisotropic behavior (AMR) which arises from ferromagnetic phase (Type I). Moreover, the GMR for x > 0.25 alloys increases steeply with annealing time t of 50 h < t < 100 h and reaches maximum (–3.6 %) for the $Ni_{0.73}Mn_{0.27}$ alloy of 693K•100 h state (Type II). While, one for x<0.25 alloys decreases slightly with t.

In Mn concentration of $0.30 \geq x \geq 0.26$, every alloy is occupied with ferromagnetic particles of about 6 nm at the rate of 50%. Nevertheless, the observed GMR varies from –0.5% to –3.5%. In order to clear this situation, we investigate an interaction between ferromagnetic particles.

5.2. Magnetization of $Ni_{1-X}Mn_X$ (x = 0.20-0.30) alloys

Fig. 9 shows the magnetization *M* vs. temperature *T* curves of $Ni_{0.80}Mn_{0.20}$, $Ni_{0.73}Mn_{0.27}$ and $Ni_{0.70}Mn_{0.30}$ alloys of 693K•100h. In Fig.9, it is seen that magnetic feature in inhomogeneous phase of the three alloys are quite different. First, saturation magnetization, M_S at 77K decreases from 59 to 14 emu g^{-1} for x = 0.20 to 0.30 with Mn concentration. Secondly, the *M*-*T* curve in Figs. 9b and 9c has a cusp in temperature range of 600K <*T* < 750K which grows with x, but in Fig.9a has not.

Fig. 10 shows the inverse susceptibility ($1/\chi$) vs. temperature curves for $Ni_{0.80}Mn_{0.20}$, $Ni_{0.73}Mn_{0.27}$ and

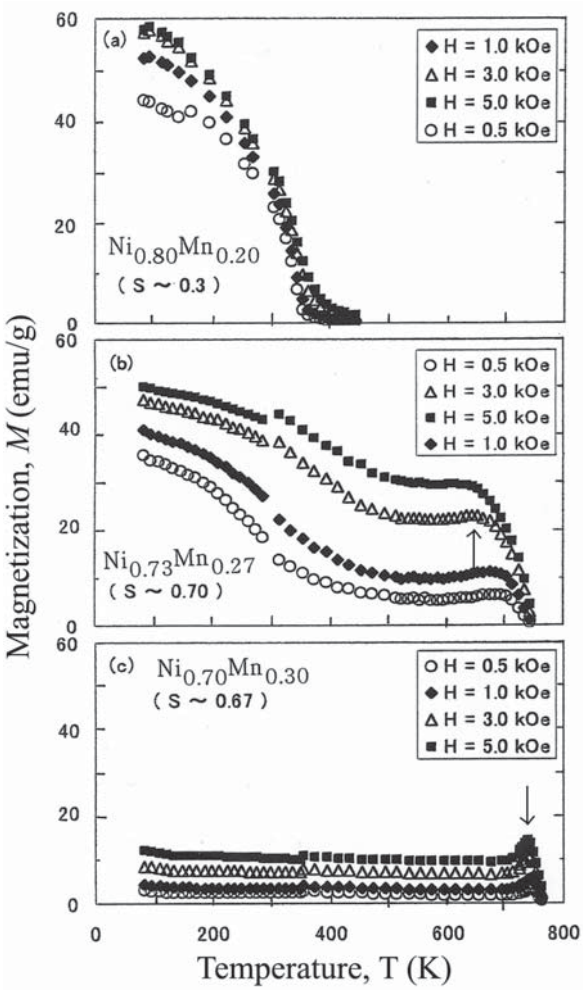

Fig. 9. Magnetization vs. temperature curves of (a) $Ni_{0.80}Mn_{0.20}$, (b) $Ni_{0.73}Mn_{0.27}$ and (c) $Ni_{0.70}Mn_{0.30}$ alloys annealed for 100 h at 693K.

$Ni_{0.70}Mn_{0.30}$ alloys at applied field of 500 Oe. The curves of $Ni_{0.73}Mn_{0.27}$ and $Ni_{0.70}Mn_{0.30}$ alloys have a minimum at 673K and 743K, respectively, that is Neel point T_N, where antiferromagnetic interaction between ordered domains disappears. While, there is no minimum in $1/\chi - T$ curve of $Ni_{0.80}Mn_{0.20}$. The paramagnetic Curie point θ_p of each alloys determined by $1/\chi - T$ curves is shown by an arrow in Fig.10.

The values of M_S, T_N, θ_p and Curie point T_F determined by Arrott plot of the present alloys are shown in Fig.11. From the results of magnetic analysis, the $Ni_{0.80}Mn_{0.20}$ alloy in which T_F is nearly equal to θ_p is found to be a typical ferromagnetic substance. There is a superparamagnetic phase between T_F and θ_p for the Ni-Mn alloys of $0.26 > x > 0.23$. The Ni-Mn alloys of $x \geq 0.26$ have T_N in high temperature range of $743K > T > 643K$, which increases with Mn concentration and is near or equal to θ_p.

5.3. Interaction between ordered domains

We think that interaction between ordered domains is caused through disordered matrix. The magnetism of Ni_3Mn depends on the number of the nearest-neighbor Mn atoms around a Mn atom [7], because a ferromagntic interaction operates for the Ni-Ni and Ni-Mn pairs and an anti-ferromagnetic one for Mn-Mn pairs. In section 4.2, we report that the inhomogeneous $Ni_{0.75}Mn_{0.25}$ alloy annealed at 693K consists of nano-scale ordered domains distributed in disordered nonmagnetic matrix (the average exchange coupling around a Mn atom, J_{ex}~0), where

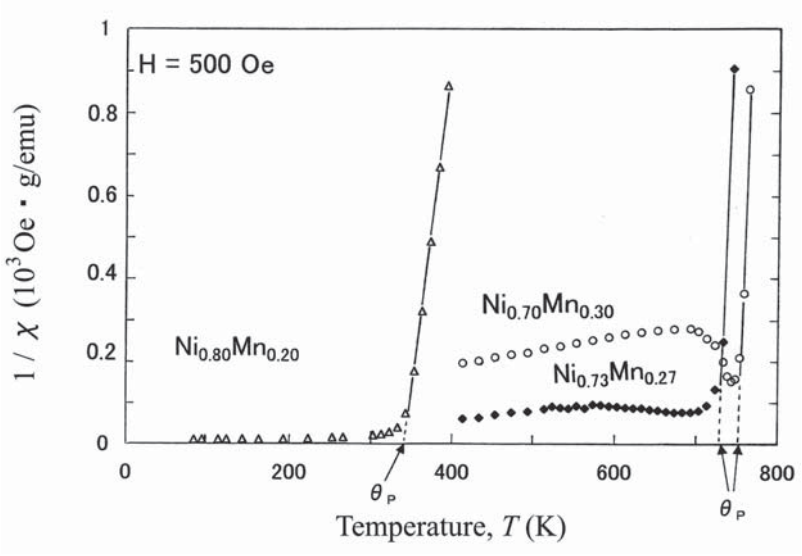

Fig.10. The inverse susceptibility ($1/\chi$) vs. temperature curves for $Ni_{0.80}Mn_{0.20}$, $Ni_{0.73}Mn_{0.27}$ and $Ni_{0.70}Mn_{0.30}$ alloys at applied field of 500 Oe.

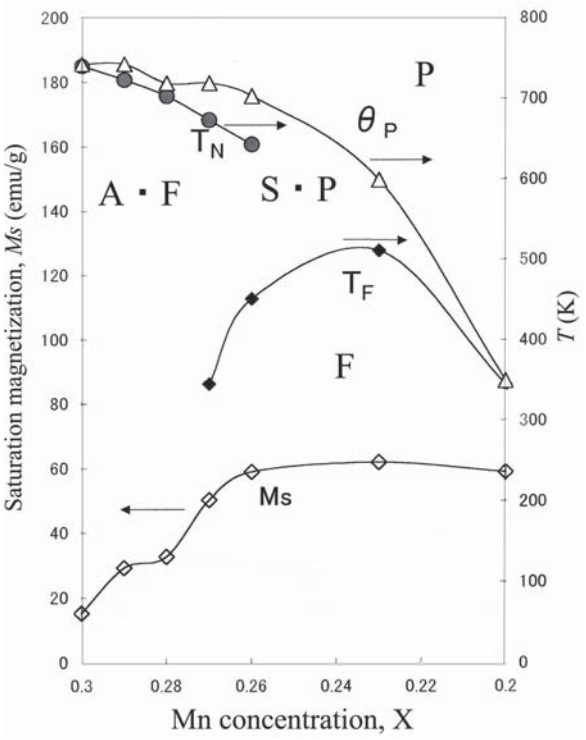

Fig. 11. Magnetic phase and Mn-concentration depensence of M_S, T_N, θ_p and T_F. There, *F*, *A•F*, *S•P* and *P* mean ferromagnetic, anti-ferromagnetic, super-paramagnetic and paramagnetic phases, respectively.

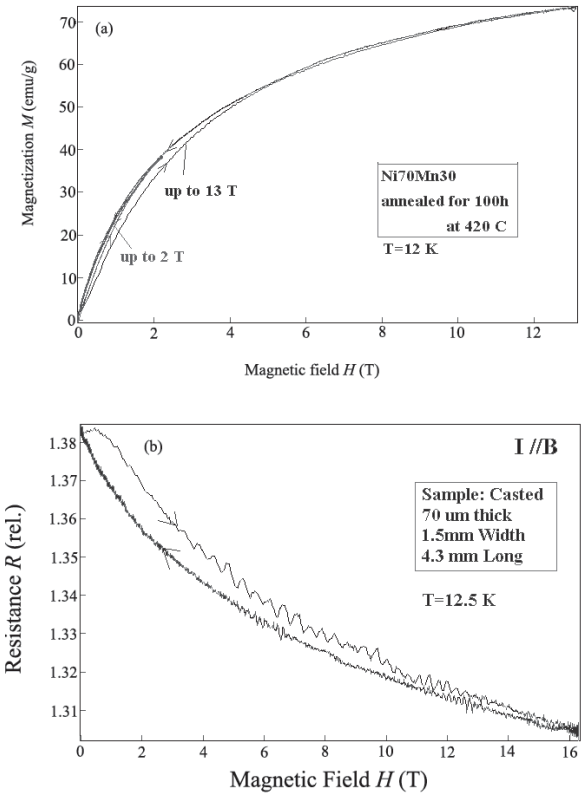

Fig. 12. Dependency of (a) magnetization and (b) GMR for $Ni_{0.70}Mn_{0.30}$ on *H* which is pulse magnetic field up to 16 T at low temperature12K.

GMR in granular ferromagnetic systems arises. The present alloys with Mn concentration of $x<0.25$ or $x>0.25$ have Ni-rich ($J_{ex}>0$) or Mn rich ($J_{ex}<0$) matrices, respectively, after super-lattice Ni_3Mn particles are precipitated and formed in the alloys.

Consequently, the ferromagnetic interaction between particles in Type I of GMR increases with decreasing *x* and makes AMR arise in MR ratio. The anti-ferromagnetic interaction between particles in Type II of GMR increases and makes M_S decrease with increasing *x*. Therefore, a maximum of GMR in Fig. 8 arises at $Ni_{0.73}Mn_{0.27}$ composition in which opposite directed domains is reversed by applied field of 10 KOe as anti-ferromagnetic interaction is weak. While, the rapidly decrease of GMR for Mn concentoration of $x>0.27$ is caused by insufficiency of applied field to reverse opposite directed domains.

From the results of magnetic analysis, Types I and II of GMR, respectively, are caused by ferromagnetic and antiferromagnetic interactions between ordered domains distributed in Ni-rich ($J_{ex}>0$) and Mn-rich ($J_{ex}<0$) matrices.

5.4. Magnetization and GMR of $Ni_{0.70}Mn_{0.30}$ alloy in magnetic field up to 16 T

Next, we investigate GMR of Ni-Mn alloys with $x > 0.25$ under high magnetic field at low temperature. Ni-Mn alloys with $x > 0.25$ at 693K•100 h state consists of ferromagnetic nano-particles(about 6 nm, $\varepsilon \sim 0.50$) dispersed in Mn-rich matrix. Since the interaction between single domains is mediated by disordered matrix, that is antiferromagnetic. Especially, antiferromagnetic interaction between nano particles for $Ni_{0.70}Mn_{0.30}$ alloy is stronger than other's one as shown in Fig.11.

Figs. 12a and 12b are dependency of magnetization and GMR for $Ni_{0.70}Mn_{0.30}$ on *H* which is pulse magnetic field up to 16 T at low temperature12K. Magnetization in Fig.12a increases rapidly with $H <$ 6T, slowly at $H >$ 6T, and then reaches to 73 $emug^{-1}$ at 13 T. The value is about 71% of that all magnetic moments of Ni and Mn atoms are parallel to applied magnetic field direction. Moreover, magnetic processes up to 2 T and down to zero are reversible.

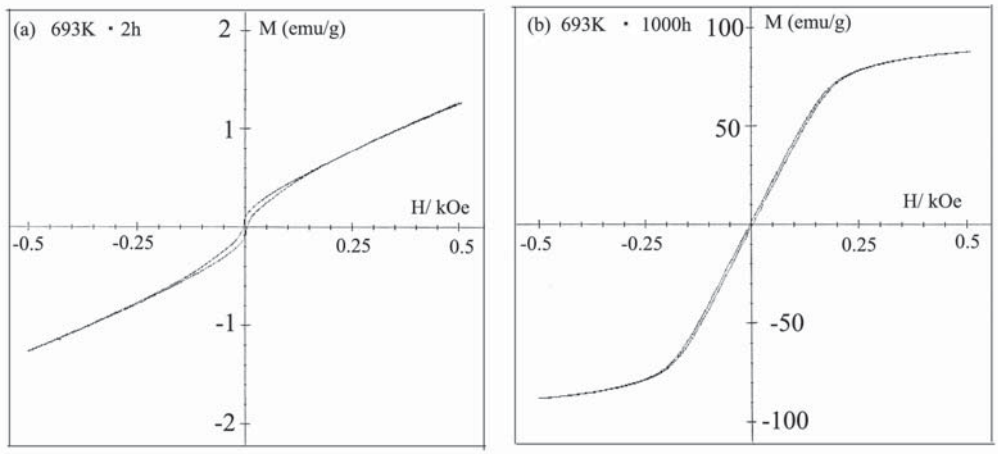

Fig. 13. The loops of magnetization vs. magnetic field for (a) 693K•2h and (b) 693K•1000 h states obtained by applied H_{max} = 500 Oe.

On the other hand, the processes up to 13 T and down to zero are irreversible.

Resistance in Fig. 12b dose not change within H < 1 T, and decreases rapidly with increasing of H. Especially, it decreases in steps as the field increases 4 T to 12 T. It is considered that the phenomenon is due to spin- flopping of single domains with various antiferromagnetic interactions. On the other hand, as the field decreases, spins rotate continuously. Consequently, GMR curve against H also has hysteresis loop.

6. SOFT MAGNETIC PROPERTY DUE TO FERROMAGNETIC NANOCRYSTAL

6.1. Coercive force of Ni_3Mn alloy

Table 1 indicates that the ferromagnetic ordered particles of the size D of 2.8~10nm distribute in a disordered nonmagnetic matrix (J_{ex}~0) in the present Ni_3Mn alloys.

In nano-scale inhomogeneous magnetic alloy, exchange and magnetic dipole interactions between particles overcome magnetocrystalline anisotropy of particles, making M_S of particle parallel to each others in one group, because the effective anisotropy constant K_{eff} is described by $K_{eff} \propto K/N$, where N is the number of particles included in one group. The coercive force H_c in nanocrystalline material can be described as [18]

$$H_c = const\ K_{eff} \frac{(D/W)^{1/2}}{M_S L}, \qquad (6.1)$$

where W and L denote a domain wall thickness and a characteristic length of exchange interaction. Assuming that W, L and M_S in Eq. (6.1) are constant, H_c is proportional to K_{eff} and $(D)^{1/2}$. Consequently, we expect soft magnetic properties in nano - scale inhomogeneous Ni_3Mn alloys.

Fig. 13 shows the M vs. H loops for (a) 693K·2h and (b) 693K·1000h states obtained by applied H_{max} = 500 Oe. The scale of M axis in (b) is 50 times of one in (a). Coercive force H_c in (a) is slightly wide, 5.5 Oe, while one in (b) becomes narrower to be 3 Oe.

The relations of H_c to annealing time t at 673 and 693K are shown in Fig. 14. It is seen that H_c for Ni_3Mn annealed at 693K shows an increase with t for 0< t <2h, a maximum, 5.5 Oe at 2h, a rapid decrease for 2h <t <5h, a minimum, 1.7 Oe at 25h and finally a slight increase up to 3 Oe at t = 1000h, where ferromagnetic particles of about 10 nm are in contact with each other. The overall t-dependence behavior of H_c for alloys annealed at 673K and 693K is rather similar, aside from the factor- of - two larger maximum of H_c, 10.7 Oe at t = 25h, for 673K – annealed alloy compared to the that for 693K – annealed alloy. The dotted line in Fig.14 displays H_c estimated from magnetoelastic energy $\lambda_S\sigma$ for 693K annealed alloy. Here, λ_S and σ are saturation magnetostriction and internal stress caused by magnetostriction λ. These H_c values are 0 ~ 2 Oe

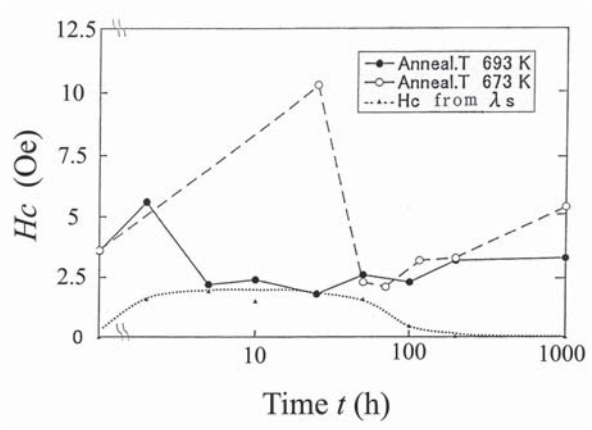

Fig. 14. Dependence of coercive force H_c on annealing time t for 673 and 693K-annealed alloys. Dotted line is estimated from magnetoelastic energy.

and can be compared with the H_c at 5< t <25h for 693K-annealed alloy (solid line). From these results, the peaking of H_c (maximum 5.5 Oe) at 2h for 693K-annealed alloy is considered to be caused by two contributions: one is H_c due to magnetostriction (~2 Oe) and the other is H_c due to internal strain of nearly completely disordered state (~3.5 Oe).

The dependence of H_c and saturation magnetic flux density B_s on ε are shown in Fig. 15, where B_s is the one measured at H_{max} = 500 Oe in Fig. 13. As seen in Fig.15, H_c rapidly increases and decreases for ε<0.1, increases gradually for 0.2 < ε < 0.8, and comes to 3 Oe. The B_s increases as the ordered region grows and reaches to 0.92 T for ε = 0.78.

However, the ε value estimated by S is uncertain in the small S range, where x-ray diffraction (110) peaks are very weak to determine S correctly as shown in Fig.2. The ε^* value of ordered region obtained by the magnetic analysis [11] is about 0.10, 0.16 and 0.32 for 693K·5h, 693K·25h and 693K·50h states, respectively.

These results indicate that the decrease of H_c for 8≤ ε ≤16 is due to the decrease of K_{eff} where magnetic particles come in contact with each other to form groups. Moreover, it is considered that the increase of H_c for ε >16% is due to the growth of D which changes 3.2 nm to 10 nm as shown in Table 1. The alloy for ε~0.8 still maintains soft magnetic properties where B_s=0.92T and H_c=3 Oe.

6.2. Soft magnetic property of $Ni_{1-x}Mn_x$ (x=0.20-0.25) alloys in high frequency range

Nano-scale inhomogeneous Ni_3Mn alloy has soft magnetic properties where the particles couple to each other ferromagenetically [21]. That is, the saturation magnetic flux density increases but the coercive force decreases with the ferromagnetic particle size.

Fig. 16 shows the dependency of H_C (H_{ext}=500 Oe) and M_C (H_{ext}=5 kOe) of wire-samples annealed for 100 h at 693K and 713K on Mn concentration. Both values depend on x remarkably. The value of H_C is small and equal to about 2.5 Oe for wire of 0.20≤ x ≤0.24, but it increases with x>0.25. It is considered that the wire of 0.24≤ x ≤0.26 annealed for 100 h at 693K consists of nano particle being almost ordered state of S=1, because their B_s equal to 1 T.

From the results, soft magnetic property due to the nanocrystalline morphology in high frequency range is expected to occur in wire of x <0.26.

Fig. 17 shows 1~500 kHz high frequency permeability of x = 0.20, 0.21, 0.24, 0.25 wires annealed for 100 h at 693K. The permeability for f =1~20 kHz is high, 200~600, but decreases slowly for f >20 kHz, because of loss due to eddy currents. To overcome these limitations, it should be necessary to prepare and study fiber or foil samples.

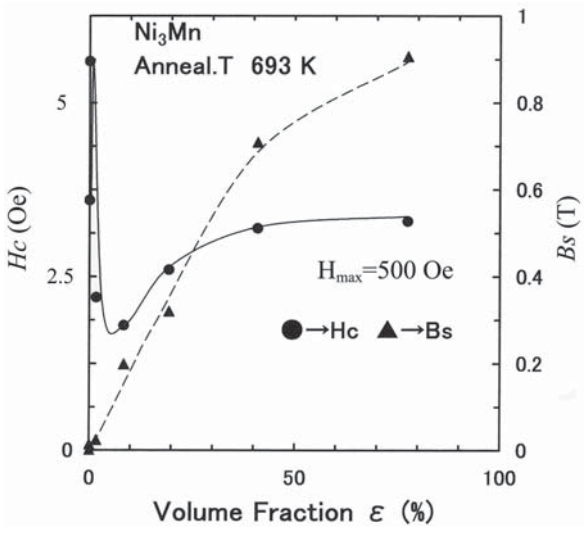

Fig. 15. Dependence of coercive force H_c and saturation magnetic flux density B_s on the volume fraction ε defined as S^2/S_{do}^2 in ordered regions.

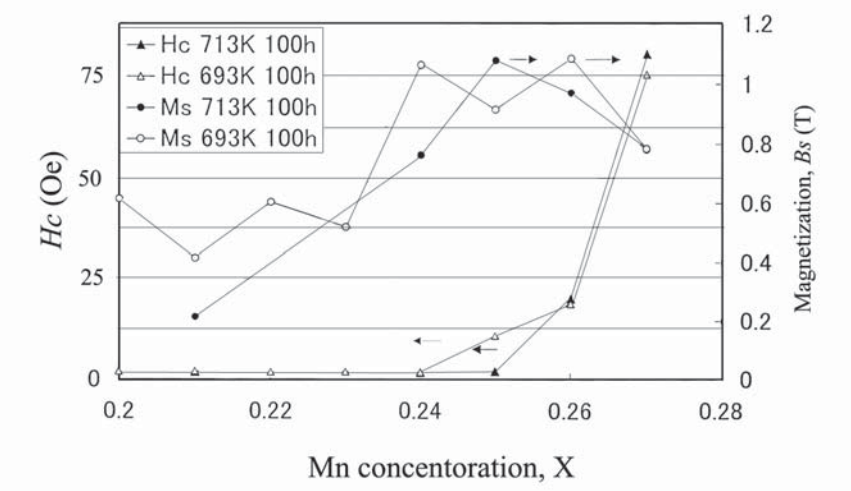

Fig. 16. Mn-concentration dependence of coercive force H_C (H_{ext}=500 Oe) and B_S (H_{ext}=5 kOe) of wire-samples annealed for 100 h at 693K and 713K.

7. CONCLUSIONS

The long-range-order parameter *S*, the magnetization and GMR were investigated for inhomogeneuos $Ni_{1-x}Mn_x$ (x = 0.20~0.30) alloys in which nano-scale ordered magnetic particles are distributed in a disordered nonmagnetic or Ni-rich or Mn-rich matrices. The main conclusions are as follows :

1. Ni_3Mn alloy with various *S*:
   The average size of ferromagnetic particle increases with the long-range-order parameter *S*, i.e., 1.4 nm to 10 nm with S = 0.13 to 0.88 . GMR depends on the volume fraction of ordered domains ε: GMR of –1.8% is obtained at ε ~ 0.27 and zero at ε ~0.8. The saturation magnetic flux density increases with ε and reaches to 0.92 T where Ni_3Mn alloy maintains soft magnetic properties due to the nanocrystalline structure.
2. $Ni_{1-x}Mn_x$ (x = 0.20~0.30) alloys annealed for 100 h at 693K:
   The values of *S*, average particle size and the volume fraction in the ordered regions are 0.3~0.7, 4~6 nm and 0.1~0.5, respectively, and increase with Mn concentration. The GMR depends remarkably on Mn concentration, x : the GMR increases from –0.5% to –1.2% for x= 0.20 to 0.24 alloys (Type I), while, for alloys of

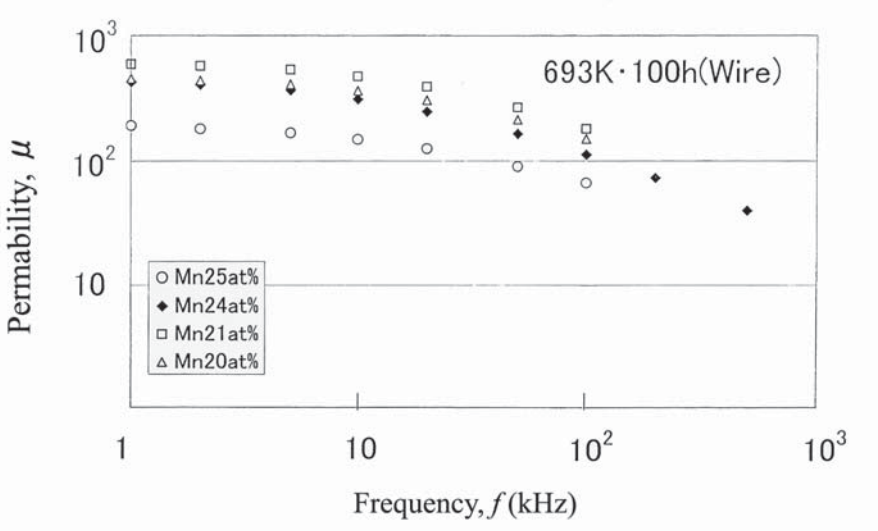

Fig. 17. High frequency permeability of $Ni_{1-x}Mn_x$(x= 0.20, 0.21, 0.24, 0.25) wires annealed for 100 h at 693K.

$0.26 \leq x \leq 0.30$, one has maximum of –6% at $x = 0.30$ at 16 T (Type II). From the results of magnetic analysis, Types I and II of GMR, respectively, are caused by ferromagnetic and antiferromagnetic interactions between ordered domains distributed in Ni-rich ($J_{ex}>0$) and Mn-rich ($J_{ex}<0$) matrices. On theother hand, $Ni_{1-x}Mn_x$ alloys of $x \leq 0.24$ exhibit soft magnetic property with permeability of 400~600 for 1~500 kHz high frequency.

REFERENCES

[1] S. Kaya and A. Kussmann // *Z. Phys.* **72** (1931) 293.

[2] S. Kaya and M. Nakayama // *Proc. Phys. - Math. Soc. Jpn* **22** (1940) 126.

[3] G. R. Piercy and E. R. Morgan // *Can. J. Phys.* **31** (1953) 529.

[4] R. Hahn and E. Kneller // *Z. Metall* **49** (1958) 426.

[5] M. J. Marcinkowski and N. Brown // *J. Appl. Phys.* **32** (1961) 375.

[6] W. Abdul-Razzaq and J. S. Kouvel // *Phys. Rev.* B**35** (1987) 1764.

[7] T. Satoh, R. B. Goldfab and C. E. Patton // *J. Appl. Phys.* **49** (1978) 3439.

[8] T. Taoka // *J. Phys. Soc. Jpn.* **11** (1956) 537.

[9] M. J. Marcinkowski and R. M. Poliak // *Philos. Mag.* **8** (1963) 1023.

[10] T. Okazaki // *Jpn Appl. Phys*. **34** (1995) 1537.

[11] T. Okazaki and Y. Kondo // *Mater. Trans. JIM*.**39** (1998) 231.

[12] K. Shiratori, E. Kita, S. Kondo and H. Ino // *J. Phys. Condens. Matter* **6** (1994) 9393.

[13] K. Shiratori, E. Kita, S. Kondo and H. Ino // *J. Phys. Condens. Matter* **6** (1994) 9405.

[14] J.Q. Xiao, J.S.Jiang and C.S.Chien // *Phys. Rev. Lett*. **68** (1992) 3749.

[15] C.S.Chien, J.Q. Xiao and J.S.Jiang // *J.Appl. Phys*. **73** (1993) 5309.

[16] K. Takahashi, T. Sugawara, K. Hono and H. Fujimori // *J.Appl. Phys*. **76** (1994) 6790.

[17] H. Fujimori, K. Takahashi, and S. Mitani // *J. Magn. Soc. Jpn.* **19** (1995) 4.

[18] H. Hoffmann // *IEEE Trans. Magn., MAG*-**9** (1973) 17.

[19] N.Hasegawa, N. Kataoka and H. Fujimori // *J. Appl. Phys.* **70** (1991) 6253.

[20] T.Okazaki, S. Sugimoto, Y. Aono, T. Miyanaga and M. Homma // *Jpn. J. Appl. Phys.* **38** (1999) 5071.

[21] T. Okazaki, K. Sawaguchi and M. Homma // *Mater. Trans. JIM.* **41** (2000) 1150.

[22] T.Okazaki, T.Miyanaga, K.Sawaguchi, Y.Sakisaka, S.Sugimoto // *J.M.M.M.* **239** (2002) 189.

[23] T.Okazaki, Y.Kumeta and Y.Sakisaka // *Mater. Trans. JIM.* **43** (2002) 2181.

[24] A. Paoletti F. P. Ricci and L. Passari // *J. Appl. Phys.* **37** (1966) 3236.

[25] J.M.Cowley // *Phys. Rev.* **77** (1950) 669.

[26] A.Paoletti and F.P.Ricci // *J.Appl. Phys.* **34** (1963) 1571.